Defect and Diffusion Forum
ISSN: 1662-9507, Vol. 450, pp 93-102
doi:10.4028/p-2lx7wD

Submitted: 2026-01-19
Revised: 2026-02-16
Accepted: 2026-02-22
Online: 2026-04-15

Static Finite Element Modeling of Milling in Flexible Composite Plates

Matthias Nutte[1,a*], Edouard Rivière-Lorphèvre[1,b], Valentin Dambly[1,2,c], Pedro-José Arrazola[3,d], Ismail Lazoglu[4,e], Aurélie Granjon[5,f] and François Ducobu[1,g]

[1]Machine Design and Production Engineering Lab, Research Institute for Science and Material Engineering, UMONS, Mons 7000, Belgium

[2]IDEKO, Dynamics & Control departement, Arriaga kalea 2, E-20870 Elgoibar, Spain

[3]Mechanical and Manufacturing Department, Faculty of Engineering, Mondragon Unibertsitatea, Loramendi 4, Arrasate-Mondragón 20500, Spain

[4]Manufacturing and Automation Research Center, Koc University, Istanbul 34450, Turkey

[5]Sobelcomp SPRL. Rue de l'économie 13, 4431 Loncin, Belgium

[a]Matthias.nutte@umons.ac.be,

Keywords: Machining, Milling, Trimming operation, Flexible parts, Composite materials

Abstract. This study presents a static finite element analysis of the milling of a flexible unidirectional glass fiber–reinforced polymer (UD-GFRP) plate. The workpiece is modeled as a clamped–free cantilever, with cutting forces evaluated independently of structural deflections and applied along the machined edge. SC8R continuum shell elements are employed to accurately represent through-thickness loading and bending behavior. A mesh sensitivity analysis is conducted to determine a suitable discretization, leading to a 64 × 56 × 8 element mesh. For the investigated configuration ($\psi = 0°$, $f_z = 0.04$mm/tooth), the out-of-plane displacement reaches approximately 120 µm near the free end of the plate, whereas in-plane displacements reach up to -75 µm. These in-plane displacements are greater than or equal to the nominal feed per tooth, indicating a highly significant influence on chip formation. This work provides a basis for understanding the structural response of flexible composite plates during trimming and emphasizes the need for coupled force–deformation formulations.

Introduction.

Fiber-reinforced polymers (FRPs) are increasingly employed in industrial applications due to their high strength-to-weight ratio, good fatigue resistance, shock absorption capacity, and strong design flexibility [1]. The forming processes of FRP components frequently lead to thin-walled geometries, making their structural flexibility a critical factor during machining operations such as trimming. These finishing operations are often required to achieve the final dimensional tolerances of molded composite parts and are still commonly performed manually. To improve process control and reduce reliance on trial-and-error approaches, it is therefore essential to accurately model the trimming process.

On the one hand, the numerical simulation of flexible metal parts has been explored in numerous studies [1, 2, 3, 4]. On the other hand, research has addressed the numerical simulation of FRP machining through comprehensive reviews [5] and cutting force modeling [6, 7]. Furthermore, specific phenomena well-documented in metal machining, such as chatter, have also been investigated experimentally in the context of composite materials [8].

Despite these advancements, to the authors' knowledge, a gap remains in the literature regarding the numerical simulation of trimming operations for flexible composite parts. While some studies have examined thin-walled composite elements experimentally [9], recent research has begun to address this by introducing numerical simulation frameworks for thinning flexible composite components[10].

The objective of this numerical study is to conduct a static analysis of the trimming process applied to a unidirectional glass fiber–reinforced polymer (UD-GFRP) composite part. The aim is to obtain a continuous displacement field of the plate, which represents the form error induced by the trimming operation. Under a simplified configuration, the workpiece is modeled as a clamped–free plate with a cantilever. Within this static framework, plate deformations are neglected in the computation of the cutting forces, which are assumed to be independent of the structural response. The plate displacement resulting from average cutting forces is then evaluated. This study is exclusively based on numerical simulations.

The static numerical methodology is first introduced through the coupling of Abaqus with a Python-based scripting framework. A mesh convergence study is subsequently carried out to assess the numerical accuracy of the model, and the simulation results are finally analyzed and discussed.

Method.

The static analysis of the trimming operation, illustrated in Fig. 1, is based on several fundamental modeling assumptions. To simplify the numerical solution and separate the prediction of cutting force from the structural response, plate deformation is neglected in the instantaneous calculation of chip thickness. The cutting tool is assumed to behave as a perfectly rigid body, whose axis remains strictly perpendicular to the initial neutral plane of the plate throughout the operation. It is also assumed that the tool operates in a pure rolling trimming configuration, which means that only the rolling teeth are engaged in the cutting operation, without any plowing effects. The structure of the machine tool is modeled as perfectly rigid, and no parasitic displacement of the tool holder or spindle is considered. The workpiece is assumed to be perfectly clamped in a vise.

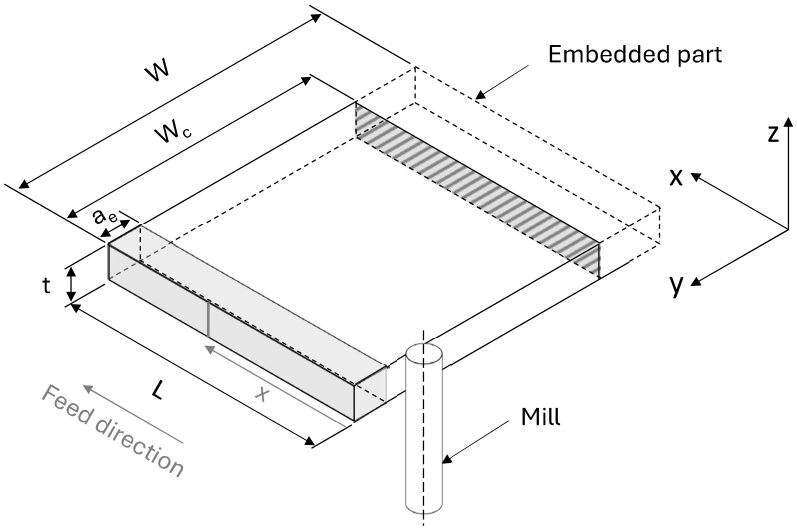

Fig. 1. Schematic representation of the configuration

The geometric parameters defining the numerical model are shown in Fig. 1. The sample is characterized by a machined length L and a cantilever length W_c, measured from the clamped area to the cutting edge. The axial cutting depth corresponds to the thickness of the sample t, while the radial cutting depth is denoted by a_e. The boundary conditions are defined by considering the shaded area inside the vise jaws as fully clamped, with all degrees of freedom constrained. The average cutting forces are applied along a vertical line corresponding to the instantaneous position of the tool x. It should be noted that these loads are applied to the unmachined edge of the plate. This choice was made to simplify the case study. The shaded volume in Fig. 1 represents the theoretical material removed during the cutting process.

The numerical implementation of the model in Abaqus is illustrated in Fig. 2. The modeled geometry corresponds to the nominal specimen dimensions, with the specimen width defined as W_c; the actual material removal is not explicitly modeled. The plate is discretized using SC8R continuum shell elements, which are eight-node hexahedral elements with three translational degrees of freedom

per node [11]. This element formulation combines the computational efficiency of shell elements with a fully three-dimensional geometric description. Unlike classical shell elements such as S4R, which discretize only the mid-surface and represent thickness through section properties [11], continuum shell elements explicitly mesh the thickness using nodes distributed along the through-thickness direction. As a result, external loads can be applied directly at discrete z-locations rather than being converted into equivalent membrane forces and bending moments acting on a reference surface. This distinction is essential for the present study. During trimming, cutting forces are transmitted to the workpiece along the contact edge between the tool and the material, where the load is intrinsically distributed across the entire thickness of the plate. The SC8R formulations allow cutting forces to be applied independently to nodes located at different positions across the thickness at the point of contact, enabling a physically consistent representation of load transfer without relying on equivalent mid-surface resultants. This capability is not available in conventional shell formulations, limiting their suitability for modeling localized loads on edges in trimming operations. The mesh density is controlled by the parameters N_x, N_y, and N_z, representing the number of elements along the longitudinal, transverse, and thickness directions, respectively. To reproduce the physical clamping conditions, the face located at $y = 0$ is subjected to a fully fixed boundary condition. The loading case is defined by the cutting forces, which are converted into equivalent nodal forces and applied to the nodes distributed along the vertical edge at the tool position x, as specified in Fig. 2.

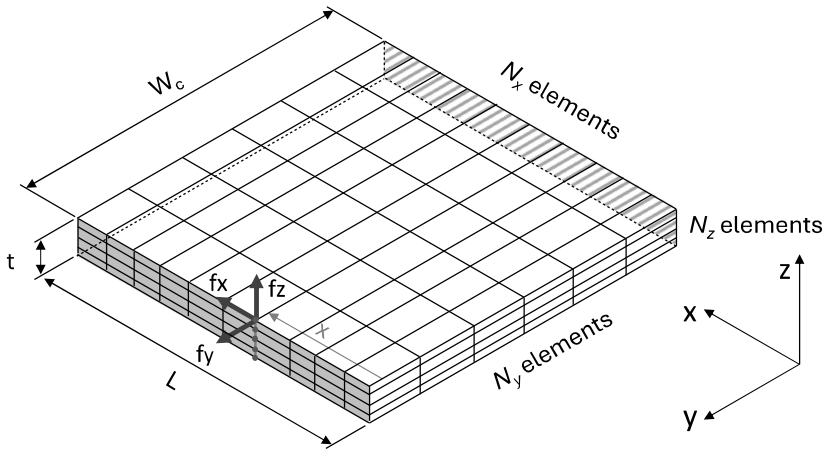

Fig. 2. Finite element model showing the applied loads and boundary conditions

As summarized in Fig. 3, the workflow begins by specifying the geometry, mesh, and boundary conditions. The setup process is fully automated through a Python script that generates the finite element model in Abaqus, allowing for total control over all modeling parameters. The resulting deformed shape is then calculated using the Abaqus Standard solver.

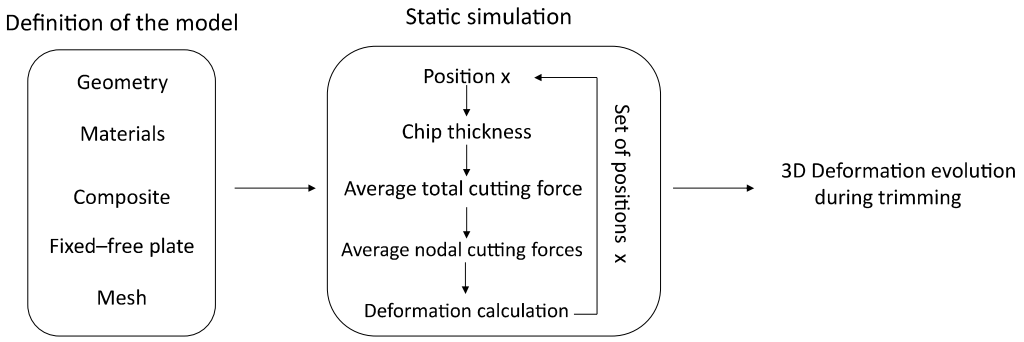

Fig. 3. Diagram of the static analysis workflow

The material behavior is modeled as a unidirectional fiber-reinforced polymer laminate. The elastic response is defined by the longitudinal Young's modulus E_1 in the fiber direction, the transverse Young's modulus E_2 in the plane perpendicular to the fibers, the shear modulus in the plane G_{12}, the out-of-plane shear moduli G_{13} and G_{23}, and the principal Poisson's ratio ν_{12}, which relates the

transverse strain in direction 2 to the longitudinal strain in direction 1. Although the formulation of the laminate allows for arbitrary stacking sequences and ply orientations, the present study focuses on a configuration in which all plies share the same fiber direction, resulting in transversely orthotropic behavior of the material throughout its thickness.

The cutting forces applied to the structure are calculated outside the finite element solver using a dedicated mechanical cutting model. This force model is based on experimentally identified specific cutting pressures and provides the full three-dimensional cutting force components. The cutting forces introduced into the finite element simulations correspond to the mean total force components (F_x, F_y, F_z) averaged over one complete revolution of the tool. Applying average forces allows the continuous value of the plate deformation to be obtained. [4]. The application of instantaneous cutting forces would require solving the dynamic response of the plate and accounting for tool–plate interaction, including the ploughing effect. This approach allows both in-plane and out-of-plane loading effects to be captured within the structural analysis. In accordance with the static framework adopted in this study, the deformations of the plate are not fed back into the cutting force calculation. Since Abaqus does not allow the direct application of continuous loads along edges, the total cutting force components (F_x, F_y, F_z) are converted into equivalent nodal forces and distributed among the nodes located along the plate thickness at the position x. Each node is therefore subjected to equivalent nodal force components (f_x, f_y, f_z) . This load transfer procedure is handled automatically by the external scripting framework. Because all unidirectional plies are aligned in the same fiber direction, identical specific cutting pressures are applied through the thickness, resulting in a uniform distribution of the equivalent nodal forces. For heterogeneous laminates or laminates with varying ply orientations, a non-uniform force distribution through the thickness could be implemented using the SC8R continuum shell formulation, which would not be feasible with conventional shell elements.

Once loading conditions are established, the Abaqus Standard solver performs a static finite element analysis to compute the displacement field. This allows for the evaluation of the three-dimensional deformation of the specimen. This analysis is repeated for all tool positions x along the cutting edge, with simulations performed only at the nodal locations of the mesh, which correspond to the discrete positions at which the cutting forces are applied. This procedure enables the reconstruction of the three-dimensional deflection of the plate throughout the trimming operation.

Cutting Force Calculation.

The cutting forces along these directions can be expressed using Eq. 1, proposed by Altintas and Lee [12]. This formulation distinguishes two types of coefficients: cutting force coefficients, which represent the specific resistance of the material to machining [13], and edge force coefficients, which account for the influence of the cutting-edge radius r_e as well as tool–workpiece interaction effects.

The cutting force coefficients K_{tc}, K_{rc}, and K_{ac} are multiplied by the axial depth of cut a_p and the uncut chip thickness h. The axial depth of cut corresponds to the depth of material engaged during a single tool pass, whereas the chip thickness represents the thickness of material removed by the cutting edge. The edge force coefficients K_{te}, K_{re}, and K_{ae} are multiplied only by the axial depth of cut a_p.

$$\begin{pmatrix} F_t \\ F_r \\ F_a \end{pmatrix} = \begin{pmatrix} K_{tc} \\ K_{rc} \\ K_{ac} \end{pmatrix} \cdot a_p h + \begin{pmatrix} K_{te} \\ K_{re} \\ K_{ae} \end{pmatrix} \cdot a_p \tag{1}$$

The cutting tool can be discretized into elementary slices along its axis of rotation. Accordingly, the total cutting forces can be decomposed into infinitesimal forces acting per tooth and per axial slice. These infinitesimal forces are expressed in Eq. 2.

The Boolean parameter g, defined in Eq. 3, takes the value 1 when the tooth is engaged with the material, i.e., when the angular position $\varphi_{j,k}$, representing the angular location of tooth j in slice k relative to the direction normal to the feed direction (also referred to as the local immersion angle), lies between the entry angle φ_{st} and the exit angle φ_{ex}. Otherwise, g is equal to 0.

$$\begin{pmatrix} dF_{t,j} \\ dF_{r,j} \\ dF_{a,j} \end{pmatrix} = g(\varphi_j)\,[\begin{pmatrix} K_{tc} \\ K_{rc} \\ K_{ac} \end{pmatrix} \cdot dz\, h_{k,j} + \begin{pmatrix} K_{te} \\ K_{re} \\ K_{ae} \end{pmatrix} \cdot dz] \tag{2}$$

$$g(\varphi_j) = \begin{cases} 1 & si\,\varphi_{st} \le \varphi_{j,k} \le \varphi_{ex} \\ 0 & otherwise \end{cases} \tag{3}$$

The uncut chip thickness generated by tooth j in slice k, denoted $h_{k,j}$, is defined by Eq. 4. It is expressed as the product of the feed per tooth f_z and the sine of the local immersion angle $\varphi_{j,k}$. The local immersion angle is determined using Eq. 5.

$$h_{k,j} = f_z \cdot \sin\varphi_{j,k} \tag{4}$$

$$\varphi_{jk} = \varphi_{10} + (j-1)\cdot\varphi_p + \frac{kdz\tan\delta}{D/2} \tag{5}$$

The immersion angle is expressed as the sum of the reference rotation angle φ_{10}, corresponding to the first contact between the first tooth and the workpiece, and the pitch angle φ_p. The pitch angle is defined as $\varphi_p = 2\pi/Z$, where Z denotes the total number of teeth. The term $\varphi_p(j-1)$ accounts for the phase shift between successive teeth. An additional term is included to account for the phase shift induced by the helix angle δ.

Once the infinitesimal tangential, radial, and axial forces are computed, they are transformed into the Cartesian coordinate system(x, y, z). In this system, the x-direction corresponds to the feed direction, the y-direction is perpendicular to the feed direction, and the z-direction is vertical. This transformation is performed using the homogeneous transformation matrix given in Eq. 6, which is valid for tools with cylindrical geometry.

$$\begin{pmatrix} dF_{xj,k} \\ dF_{yj,k} \\ dF_{zj,k} \end{pmatrix} = \begin{bmatrix} -\cos\varphi_{j,k} & -\sin\varphi_{j,k} & 0 \\ \sin\varphi_{j,k} & -\cos\varphi_{j,k} & 0 \\ 0 & 0 & 1 \end{bmatrix} \cdot \begin{Bmatrix} dF_{tj,k} \\ dF_{rj,k} \\ dF_{aj,k} \end{Bmatrix} \tag{6}$$

The specific cutting pressures are defined as second-order Fourier series ($M = 1$) depending on the instantaneous fiber cutting angle θ, as expressed in Eq. 7 [7].

$$K_{pq}(\theta) = \sum_{i=0}^{M}\left(C_i^{pq}\cos(2i\theta) + S_i^{pq}\sin(2i\theta)\right) \quad \text{avec} \quad p = t, r, a; q = c, e \tag{7}$$

The values of the constants, experimentally identified for the considered material and cutting tool, are reported in Table 1 [7].

Table 1. Cutting coefficients constant

Coefficient	K_{tc}	K_{rc}	K_{ac}	K_{te}	K_{re}	K_{ae}
C_0	255.7	353.4	48	6.2	1.6	0.1
C_1	7.6	-16.4	−30.7	-1.2	7	0
S_1	16.4	7.6	6.6	11.1	2.1	0

Numerical setup.

In the framework of this study, the cutting conditions, tool characteristics, and material properties used as input data for the numerical model are summarized as follows. The investigated material is a unidirectional glass fiber-reinforced polymer (UD-GFRP), whose orthotropic elastic behavior is fully characterized by six independent constants. The longitudinal Young's modulus E_1 = 39,000 MPa reflects the stiffness in the fiber direction, while the transverse modulus E_2 = 8,600 MPa characterizes the matrix-dominated response perpendicular to the fibers. The in-plane shear modulus G_{12} = 3,800 MPa governs the shear behavior within the laminate plane, and the out-of-plane shear modulus G_{13} is assumed equal to G_{12}. The transverse shear modulus G_{23} = 1,900 MPa is estimated as half of G_{12} following the approach proposed in [14]. The principal Poisson's ratio ν_{12}= 0.28 relates the transverse strain to the longitudinal strain under uniaxial loading in the fiber direction. The laminate is composed

of 14 unidirectional plies, all oriented in the same direction. These material properties were provided by Sobelcomp. The plate geometry is defined by a length L of 80 mm, a cantilever length W_c of 75 mm, and a thickness t of 7.2 mm. The fiber orientation is uniform throughout the laminate and corresponds to an angle $\psi = 0°$ for all plies. The fibers are oriented parallel to the feed direction. This configuration was selected to minimize the occurrence of defects in the surface plies [15]. Machining is performed using a 6 mm diameter (D_c), four-flute carbide milling cutter featuring a 10° helix angle, specifically designed for machining thermoset or thermoplastic G/C-FRP materials (Reference Seco Tools: 880060R020Z4.0-DURA). The cutting parameters, including the axial a_p and radial a_e depths of cut (ap = t = 7.2 mm; ae = D_c/2 = 3 mm), the cutting speed (v_c = 125 m/min), and the feed per tooth (f_z = 0.04 mm/th), are selected in accordance with the recommendations of the tool manufacturer, Seco Tools, to ensure representative and industrially relevant machining conditions. These parameters constitute the complete set of input data used both for the calculation of the cutting forces and for the subsequent static finite element simulations.

Results.

Mesh convergence.

SC8R continuum shell elements are specifically designed to handle high aspect ratios between in-plane dimensions and thickness [11]. This characteristic makes them well-suited for modeling thin plate-like structures where element dimensions in the plane significantly exceed the through-thickness dimension. However, accurate resolution of bending behavior requires multiple elements stacked through the thickness. Since each SC8R element contains only a single integration point, using only one element through the thickness would lead to nonphysical results, particularly in bending-dominated configurations.

The plate considered in this study has dimensions of 80 mm × 75 mm × 7.2 mm. To ensure consistent element quality across mesh refinement levels and to provide adequate through-thickness resolution, a proportional mesh refinement strategy is adopted. The mesh is refined uniformly in all spatial directions while maintaining constant aspect ratios between refinement levels, to limit the influence of element aspect ratio on the numerical results and isolate the effect of mesh density. For the convergence study, four refinement levels are considered, with a fixed refinement ratio of 2 between successive levels. The corresponding mesh configurations are summarized in Table 2. All mesh configurations maintain moderate through-thickness aspect ratios (dx/dz = 1.39, dy/dz = 1.49) and in-plane aspect ratios close to unity (dx/dy = 0.93). The use of at least two elements through the thickness in the coarsest mesh ensures that bending gradients are captured, while finer meshes provide progressively improved resolution and numerical accuracy.

Table 2. Mesh configurations for convergence study

Level	N_x	N_y	N_z	# Elements	dx [mm]	dy [mm]	dz [mm]
1 – Coarse	16	14	2	448	5	5.36	3.60
2 – Medium	32	28	4	3584	2.5	2.68	1.80
3 – Fine	64	56	8	28672	1.25	1.34	0.90
4 – Very fine	128	112	16	229376	0.625	0.67	0.45

The convergence analysis is performed by monitoring the normalized displacements U_1^*, U_2^*, U_3^*, and the total displacement U_{tot}^*, evaluated at a reference node located at the center of the plate, on the middle surface, corresponding to $x = 0$ mm. The displacement values are normalized with respect to those obtained using the coarse mesh. The results, presented in Fig. 4, show that increasing the mesh density has a significant influence on the in-plane displacement components U_1^* and U_2^*, while U_3^* and U_{tot}^* exhibit similar convergence trends. It is important to note that the orders of magnitude of U_1 and U_2 differ from those of U_3 and U_{tot}, which explains why the strong evolution of U_1^* and U_2^* has a limited impact on the total displacement. Beyond a certain refinement level, further increases in mesh density have a negligible effect on U_{tot}, indicating that a very fine mesh is not required for accurate prediction of global deflection. Nevertheless, a sufficiently refined mesh remains necessary to

accurately capture the in-plane displacement components. It is also observed that the out-of-plane displacement U_3 is overestimated when using the coarsest mesh, which employs only two elements through the thickness. This confirms that more than two through-thickness elements are required to properly represent bending behavior.

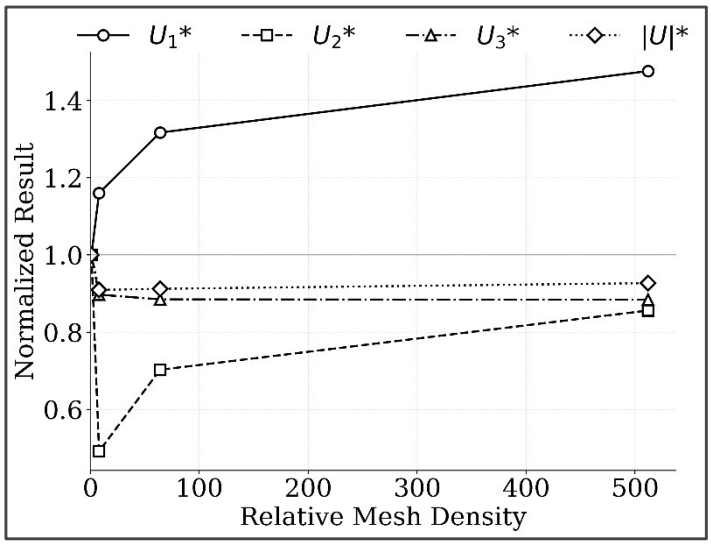

Fig. 4. Mesh convergence of normalized displacements at the reference node

The relative computation time associated with each mesh configuration is shown in Table 3. All simulations were performed on a desktop workstation equipped with an Intel Core i5-6400 processor (4 cores, 2.70 GHz) and 16 GB of RAM, running Windows 10 Pro 64-bit. Adding more elements in the longitudinal direction has a double impact on the calculation time. Not only does it increase the cost of each single simulation, but it also increases the total number of simulations required, since an analysis is performed at every nodal point along the tool path. From a computational standpoint, the very fine mesh is therefore not viable, as it leads to computation times approximately 200 times longer than those of the coarse mesh (approximately 15 seconds). Considering both numerical accuracy and computational efficiency, the fine mesh configuration, defined by $N_x = 64$, $N_y = 56$, and $N_z = 8$, is selected for the remainder of the study. This choice provides an appropriate compromise between solution accuracy and computational cost.

Table 3: Computational cost of mesh configurations for convergence study

Level	U1 [µm]	U2 [µm]	U3 [µm]	|U| [µm]	Relative unit time	Relative total time
1 – Coarse	-34.5	-17.7	140.3	145.6	1.0	1.0
2 – Medium	-40.0	-8.7	125.9	132.4	1.2	2.3
3 – Fine	-45.4	-12.4	124.2	132.8	2.7	10.2
4 – Very fine	-50.9	-15.1	124.1	134.9	26.3	199.7

Results.

Figure 5.a presents the averaged cutting forces calculated for the investigated configuration. Since the current model does not account for plate deformation in the computation of the chip thickness, the cutting forces remain constant over the entire range of plate positions along the x-direction. The in-plane force components are dominant. The longitudinal force F_x is the largest component, with a magnitude of approximately −141 N, while the transverse force F_y reaches about 44 N. The out-of-plane force component F_z is positive and significantly smaller, with a value of approximately 12 N. In this configuration, F_z represents only about 8.5% of the magnitude of the dominant longitudinal force.

Figure 5.b presents the displacement components U_1, U_2, and U_3, corresponding to the x-, y-, and z-directions, respectively, for the investigated configuration ($f_z = 0.04$ mm). The plate exhibits a pronounced out-of-plane displacement U_3 at the free ends, which is consistent with the behavior of a

cantilever subjected to edge-applied loads. This out-of-plane component reaches a maximum magnitude of approximately 120 μm near the plate extremities ($x = 0$ and $x = 80$mm) and gradually decreases toward the center, attaining a minimum value of about 70 μm at mid-span. The in-plane displacements, although smaller than U_3, remain significant. The longitudinal displacement U_1ranges from approximately −30 μm at mid-span to −75 μm near the extremities. The transverse displacement U_2varies between approximately −20 μm and 30 μm along the trimming path. While U_3remains the largest individual displacement component, the total displacement magnitude is substantially influenced by the longitudinal deformation, which is of the same order of magnitude.

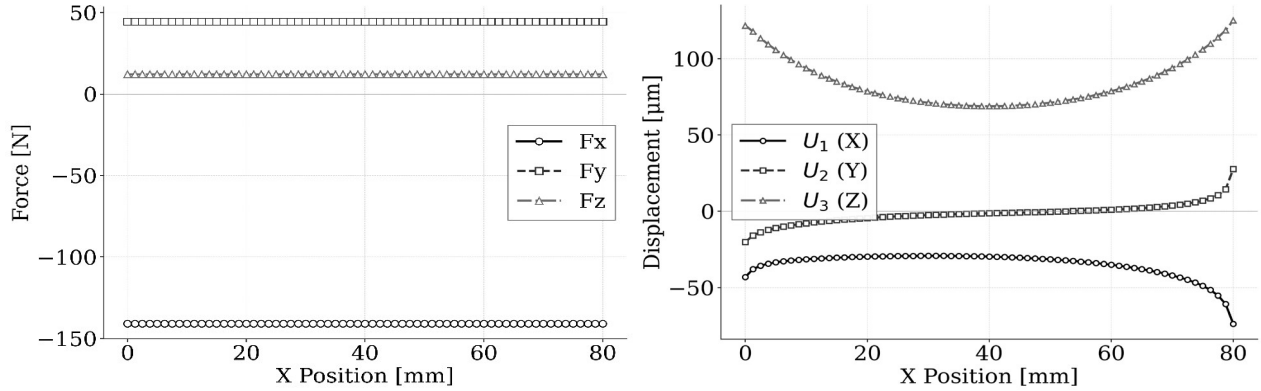

Fig. 5. a) Average cutting force; b) Displacement $\boldsymbol{U_1}$, $\boldsymbol{U_2}$, and $\boldsymbol{U_3}$ at the loaded edge

Despite the out-of-plane cutting force $F_z$being the smallest component (approximately 12 N), the resulting displacement U_3remains the dominant structural response. This behavior is characteristic of thin cantilever plates, for which the bending stiffness is significantly lower than the in-plane membrane stiffness. In addition, with fibers oriented at 0°, the bending stiffness associated with out-of-plane deformation is governed primarily by the transverse Young's modulus E_2, which is significantly lower than the longitudinal modulus E_1.

The out-of-plane displacement, reaching approximately 120 μm at the plate extremities, induces local plate rotations that may alter the effective tool–workpiece engagement geometry. The in-plane displacements $U_1$and U_2have a more direct influence on chip formation. In particular, U_1, which reaches up to 75 μm, exceeds the nominal feed per tooth ($f_z = 40$ μm) near the plate ends, potentially leading to a substantial modification of the instantaneous chip thickness. Meanwhile, U_2directly affects the radial depth of cut. These observations underline the necessity of coupled formulations that explicitly account for the strong interaction between structural deformation and cutting mechanics.

Conclusion.

A static finite element methodology has been developed to predict milling-induced deflections in a flexible UD-GFRP plate. SC8R continuum shell elements provide an appropriate framework for modeling edge-applied cutting loads with through-thickness distribution, enabling physically consistent load transfer without relying on equivalent mid-surface resultants. A preliminary mesh convergence study indicates that a 64×56×8 element configuration offers a reasonable balance between numerical accuracy and computational cost, with at least four elements through the thickness necessary to capture bending behavior. For the studied configuration (ψ = 0°, f_z = 0.04 mm/th), the out-of-plane displacement U_3 reaches 120 μm near the plate extremities where structural stiffness is reduced, while in-plane displacements remain one order of magnitude smaller. Although smaller in magnitude, the in-plane displacements have direct implications for cutting mechanics: the longitudinal displacement U_1 ranges from -30 to -75 μm, making it comparable to or even larger than the nominal feed per tooth. This directly affects the chip thickness, while the transverse displacement U_2 (up to 30 μm) modifies the radial depth of cut. The out-of-plane displacement induces local plate rotation that may affect the effective tool-workpiece engagement geometry. The current approach

neglects the feedback of plate deformation on cutting forces, assumes perfectly rigid clamping, and does not account for material removal or dynamic effects. Future work will address semi-static simulations incorporating the influence of plate deformation on chip thickness, multi-directional laminates with non-uniform force distributions through the thickness, and experimental validation. A dynamic simulation should also be considered. This would allow instantaneous forces to be applied to the plate instead of average forces, as is currently done. This study provides a foundation for predicting and controlling the structural response of flexible composite components during machining operations, but further experimental investigations are necessary to validate the numerical results.

Acknowledgments

The authors would like to thank Région Wallonne for supporting this research as part of the MachFlexComp M-ERA.NET 2022 research project under grant 2210138.

References

[1] I. Llanos, A. Robles, J. Condón, M. Arizmendi, and A. Beristain, 'Deflection error modeling during thin-wall machining', *Procedia CIRP*, vol. 117, pp. 169–174, 2023, doi: 10.1016/j.procir.2023.03.030.

[2] I. Del Sol, A. Rivero, L. N. López de Lacalle, and A. J. Gamez, 'Thin-Wall Machining of Light Alloys: A Review of Models and Industrial Approaches', *Materials*, vol. 12, no. 12, Art. no. 12, Jan. 2019, doi: 10.3390/ma12122012.

[3] A. Hussain and I. Lazoglu, 'Distortion in milling of structural parts', *CIRP Annals*, vol. 68, no. 1, pp. 105–108, 2019, doi: 10.1016/j.cirp.2019.04.053.

[4] E. Rivière-Lorphèvre, E. Filippi, and P. Dehombreux, 'Numerical Simulation of Machining Operations on Flexible Parts', *KEM*, vol. 554–557, pp. 1984–1991, Jun. 2013, doi: 10.4028/www.scientific.net/KEM.554-557.1984.

[5] J. Du, M. Geng, W. Ming, W. He, and J. Ma, 'Simulation machining of fiber-reinforced composites: A review', *Int J Adv Manuf Technol*, vol. 117, no. 1–2, pp. 1–15, Jul. 2021, doi: 10.1007/s00170-021-07531-3.

[6] Y. Song, H. Cao, W. Zheng, D. Qu, L. Liu, and C. Yan, 'Cutting force modeling of machining carbon fiber reinforced polymer (CFRP) composites: A review', *Composite Structures*, vol. 299, p. 116096, Nov. 2022, doi: 10.1016/j.compstruct.2022.116096.

[7] M. Nutte *et al.*, 'Mechanistic modeling of cutting forces in milling of unidirectional Glass Fiber Reinforced Polymer (UD-GFRP)', *Procedia CIRP*, vol. 133, pp. 424–429, 2025, doi: 10.1016/j.procir.2025.02.073.

[8] K. Kecik, R. Rusinek, J. Warminski, and A. Weremczuk, 'Chatter control in the milling process of composite materials', *J. Phys.: Conf. Ser.*, vol. 382, no. 1, p. 012012, Aug. 2012, doi: 10.1088/1742-6596/382/1/012012.

[9] K. Ciecieląg and K. Zaleski, 'Milling of Three Types of Thin-Walled Elements Made of Polymer Composite and Titanium and Aluminum Alloys Used in the Aviation Industry', *Materials (1996-1944)*, vol. 15, no. 17, p. 5949, Sep. 2022, doi: 10.3390/ma15175949.

[10] M. Nutte, Rivière-Lorphèvre, Edouard, Dambly, Valentin, Arrazola, Pedro-José, Lazoglu, Ismail, and Ducobu, François, 'Numerical simulation of milling operations on flexible composite parts', presented at the Material Forming, May 2024, pp. 2041–2049. doi: 10.21741/9781644903131-225.

[11] Dassault Systèmes, ‘About Shell Elements’, in *Abaqus Elements Guide*, Dassault Systèmes. Accessed: Jan. 19, 2026. [Online]. Available: https://docs.software.vt.edu/abaqusv2024/English/?show=SIMACAEELMRefMap/simaelm-c-shelloverview.htm

[12] Y. Altintaş and P. Lee, ‘A General Mechanics and Dynamics Model for Helical End Mills’, *CIRP Annals*, vol. 45, no. 1, pp. 59–64, Jan. 1996, doi: 10.1016/S0007-8506(07)63017-0.

[13] Y. Karpat, O. Bahtiyar, and B. Değer, ‘Mechanistic force modeling for milling of unidirectional carbon fiber reinforced polymer laminates’, *International Journal of Machine Tools and Manufacture*, vol. 56, pp. 79–93, May 2012, doi: 10.1016/j.ijmachtools.2012.01.001.

[14] C. L. Tsai and I. M. Daniel, ‘Determination of in-plane and out-of-plane shear moduli of composite materials’, *Experimental Mechanics*, vol. 30, no. 3, pp. 295–299, Sep. 1990, doi: 10.1007/BF02322825.

[15] Kevin Colligan and Mamidala Ramulu, ‘The effect of edge trimming on composite surface plies’, *Manufacturing Review*, vol. 5, no. 4, pp. 271–283, Dec. 1992.

The publication of this article was funded by the Mondragon Goi Eskola Politeknikoa, J.M.A. S.Coop